Charge dynamics following high-intensity laser propagation through gas jet targets

S Kar, M Borghesi, L Romagnani, C A Cecchetti

Department of Physics and Astronomy, Queen's University of Belfast, Belfast, BT7 1NN, UK

R Jung, J Osterholtz, O Willi

Heinrich Heine Universitat Dusseldorf, Dusseldorf, Germany

J Fuchs

LULI, Ecole Polytechnique, Palaiseau, France

A Macchi

INFM and Physics Department, University of Pisa, Pisa, Italy

T V Liseykina

Theoretische Physik Institute, Ruhr-Universitaet, Bochum, Germany

A Schiavi

Department of Physics, University of Rome, Rome, Italy

M Galimberti, L A Gizzi

IPCF-CNR, Pisa, Italy

R Heathcote, D Neely

Central Laser Facility, CCLRC Rutherford Appleton Laboratory, Chilton, Didcot, Oxon., OX11 0QX, UK

Main contact email address: *s.kar@qub.ac.uk*

Introduction

The study of the propagation of an intense laser pulse through under-dense plasmas is relevant to a wide range of applications, including laser driven electron acceleration[1-6] and the fast ignitor scheme for inertial confinement fusion[7]. These application areas demand a detailed study of mechanisms such as laser plasma channelling[7,8], self-focussing[9,10] and the dynamics of the plasma channels caused by coulomb explosion[11]. However, a driving force in this field of research has also been the desire of testing a class of new physical phenomena in the strong nonlinear regime attained by ultrahigh intensity laser plasma interactions, only recently made possible by the progress of the laser technology.

The development of the proton imaging technique[12] has provided additional capabilities to explore the dynamics of laser plasma interaction by detecting the associated transient electromagnetic field structures. Employing this technique, the interaction of a high intensity laser with an underdense plasma was studied in a recent experimental campaign at the Rutherford Appleton Laboratory. The results not only demonstrate the uniqueness and novelty of the diagnostic technique but also provide a deep insight into the fundamental physical processes involved, which had so far only been inferred from particle in cell simulations. In this report, we are presenting the results and modelling relating to the early stage of nonlinear laser plasma interaction with some preliminary interpretation of later time developments.

Experimental Setup

The experiment was carried out at the Rutherford Appleton Laboratory, employing the 100 TW Nd-Glass Vulcan laser operating in the Chirp Pulse Amplification mode. The dual CPA configuration previously used in these types of experiments was employed, providing two CPA pulses with adjustable relative delays. Each of the output beams delivered approximately 50 J in 1.2 ps (FWHM) duration. By using off-axis parabolas, the beams were focused down, on different targets, to spots of 10 µm FWHM, with peak intensity reaching about 1.5×10^{19} W/cm². One of the beams interacted with the He gas from a supersonic nozzle driven at 50 bar pressure. Different intensities were achieved by inserting neutral density filters in the beam, before the compressor. The other CPA beam was employed to generate the probe proton beams by irradiating it onto a flat foil (a 10 µm thick Au foil was typically used). Proton beams were observed having a quasi-Maxwell Boltzmann energy spectrum with temperature and cut-off energy of 3 MeV and 18 MeV respectively. The detector was a multilayered Radio-chromic film (RCF) detector, placed at a distance of 2-3 centimetres from the gas jet. In the condition of the experiment, this provided a multi-frame temporal scan of the interaction for up to 50 ps in a single shot[12]. The temporal resolution of each frame was typically of the order of few picoseconds, predominantly depending upon the transit time of the protons through the interaction region. The time of arrival of the protons of a given energy at the interaction point was controlled by a double pass timing slide, inserted in the path of CPA1, before amplification, with ps resolution. The point projection magnification was approximately 11. The spatial resolution in our case can be assumed to be of the order of 5-10 of microns, which is the typical dimension of the virtual source of the protons[13].
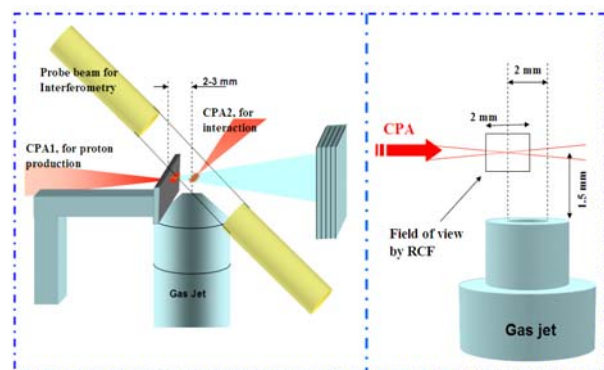

Figure 1.   (a) Schematic of the experimental setup. (b) view of the setup from different angle (normal to proton generating foil), showing the position of laser focus with respect to the field of view of proton imaging diagnostics.

The interaction was also probed by simultaneously operating Nomarsky interferometry and shadowgraphy diagnostics, employing a frequency doubled CPA probe pulse of low energy. The arrival of the CPA1 and optical probe at the interaction point was synchronised with few ps precision with

an optical streak camera. The main purpose of this diagnostic was to obtain the pre-plasma conditions ahead of the short pulse. *KODAK HP5* films were used to record the interferograms and shadowgraphs at a magnification of 85 and 55 respectively. The layout of the setup and the field of view of the proton imaging diagnostics are shown in Figure 1. The temporal and spatial neutral gas density profile, at different pressure, for the supersonic nozzle of *Mach number* 3.5 was measured via interferometric technique. The details of this work can be found elsewhere[14].

Pre-plasma Characterisation:

The interferograms and shadowgraphs of the pre-plasma, taken at few tens of picoseconds before the arrival of the main pulse at its focal plane (henceforth, referenced as t = 0) provided the absolute measurement of the plasma density over the interaction region as shown in Figure 2. Interestingly, this data shows the presence of a plasma channel with double boundaries, which is currently under process of analysis. Preliminary studies with hydrodynamic simulation POLLUX have revealed dual channel boundaries of the same dimension in the case of a flat top prepulse of expected intensity and duration.
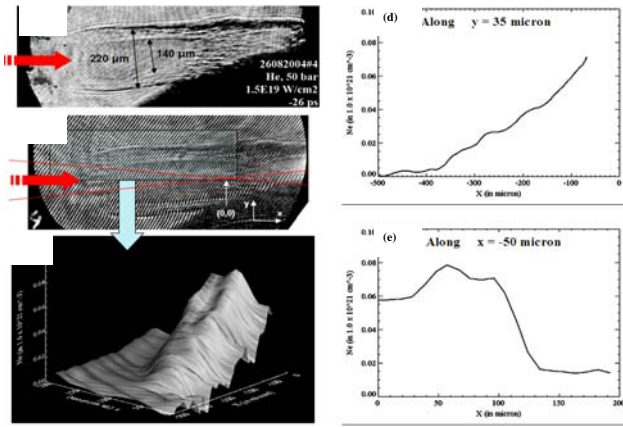

Figure 2. (a) and (b) are the shadowgraph and interferogram of the plasma at 25 picoseconds before the arrival of the short pulse at the focus (denoted by the coordinate (0, 0) in (b)). He gas pressure was 50 bar and the peak intensity of the laser was 1.5×10^{19} W/cm^2. The electron density profile obtained from the interferogram is shown over the transverse plane (c) and along two different axes [(d) and (e)].

Interaction of short pulse with the under-dense plasma:

The interaction of the high intensity short pulse laser with the under-dense plasma was observed for a few hundreds of picoseconds, starting from the time of entry of the laser into the field of view of the proton beams. To the best of our knowledge, this represents the first time-resolved measurement of the space-charge electric fields generated during the interaction. Several interesting physical phenomena were observed during the comprehensive study of the interaction at different gas pressure (giving rise to different density of the under-dense plasma) and different intensities of the laser.

(i) Early phase of Interaction:

The entry of the short pulse into the field of view and its propagation through the plasma was observed via the generation of an electron depleted ion channel due to the strong radial ponderomotive force of the laser, exerted on the plasma electrons. The positively charged ion channel deflects the probe protons outward from the laser axis along the radial direction, creating a 'negative' shadow of the channel over the RCF. Figure 3 shows the proton images obtained at two early times of interaction, for two different laser intensities.

The proton images of the ion channel show three different characteristic features at different regions, corresponding to different stages of the interaction. They are **(1)** a 'bullet' shaped channel, **(2)** a 'white' channel (corresponding to lower probe proton flux than the background) with sharp black boundary, and **(3)** a *white* channel with a dark line on axis.
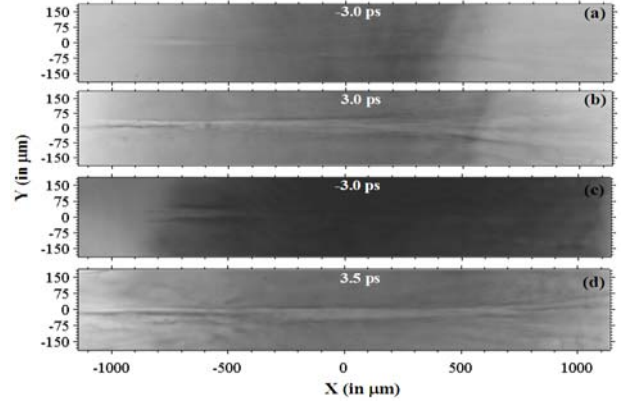

Figure 3. The proton images showing different times of interaction of a laser pulse having peak intensity nearly equal to 4.0×10^{18} W/cm^2 [(a) and (b)] and 1.5×10^{19} W/cm^2 [(c) and (d)].

Since the density of the matter is too low for significant scattering of the probe protons in the region under observation, the modulation in the optical density, imprinted over the RCF, and across the channel will mainly depend on the radial electric field profile. We neglect the effect of the magnetic field for the sake of simplicity. Presuming the dominant mechanism behind the observed phenomena is the radial ponderomotive expulsion of the electrons [15, 16] with static ions, an analytical expression for the radial electric field can be derived by considering the problem as cylindrically symmetrical, which is given by

$$E_R(\xi) = \frac{m\omega_p c}{2^{3/2} e} \frac{\xi}{\xi_0^2} \frac{a_0^2 e^{-\frac{\xi^2}{\xi_0^2}}}{\sqrt{2 + a_0^2 e^{-\frac{\xi^2}{\xi_0^2}}}} \qquad (1)$$

where, $\omega_p = \left[\frac{4\pi n_0 e^2}{m}\right]^{1/2}$, $\xi = \frac{r\omega_p}{c}$, $\xi_0 = \frac{r_0 \omega_p}{c}$ and a_0 is the laser strength parameter.

From the above expression of the radial electric field, it is evident that the intensity of the electric field is a function of both plasma density and laser intensity. Using this expression, the channel was modeled in the particle tracing code, PTRACE. The plasma density profile, as obtained from the interferograms, and the non-uniform laser beam size over the field of view of RCF were considered in the simulation. The particle tracing through the channel was carried out for different positions of the laser pulse in the field of view, which produced the 'bullet' like image for the front end of the channel, as shown in the Figure 4. However, the tip of the 'bullet' does not always correspond to the position of the leading edge of the pulse. This is likely to be due to the existence, for each proton energy, of a threshold in electric field below which the proton deflection and the consequent RCF optical density variation are not significant.

The effect of the laser self-focusing has not been considered in the above analytical treatment. However, for each case it was observed that the tip of the 'bullet' corresponds to a slice of the pulse where $I_0 \times \pi r^2$ is less than the critical power required for the self-focusing, at least by a factor of 10.

Behind the 'bullet' shaped tip, the "white" channel in the RCF optical density results from proton deflection from a radial, outwardly-directed electrostatic field due to charge separation. The variation of the radial field along the axis at a fixed time and the laser pulse motion during the temporal duration of the proton snapshot account for the channel length (up to 750 µm) observed in the data.
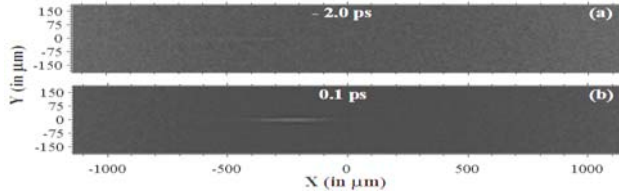

Figure 4. Proton images of the channel produced by PTRACE simulation at two different times for the laser peak intensity is 4×10^{18} W/cm^2 and 10 µm FWHM spot size at focus. The analytical formula given by Equation (1) has been used to model the channel in the simulation.

The third interesting feature observed in the proton images during the early phase of interaction is the piling up of the probe protons along the axis of the channel giving a dose profile across the channel having a peak at the centre of a 'white' region. The distribution of the dose suggests the presence of a radial electric field changing sign along the radius (i.e. inwardly directed close to the axis and outwardly directed at larger distances from it).

A qualitative explanation of the mechanisms taking place after the interaction can be given as follows. Ions inside the electron depleted channel, created by the ponderomotive expulsion of the electrons during the presence of the laser beam, gain momentum radially in the outward direction and start moving accordingly. The process is well known as Coulomb explosion. In this way, the radial ion density will be depleted on the axis of the channel and therefore will create a finite width 'wall' at some radial position depending on time. After the laser pulse, since there is no more ponderomotive force acting on them, electrons will return back into the channel to shield the ion species in order to retain the quasi-neutrality condition. Due to the heavy mass, ions will be insignificantly affected by the return of electrons. As a matter of fact, due to the high temperature of the electrons, gained by the laser ponderomotive force, they will not be efficient to shield the ion 'wall' by virtue of their overshooting oscillation. Beneath the wall, towards the axis, their excess charge density will generate a negative electric field which can be seen as the reason of the formation of the central black line along the axis of the channel.

A one dimensional relativistic, electrostatic particle-in-cell simulation code has been developed in cylindrical coordinate system to investigate the two-species charge dynamics. The code solves the relativistic equation of motion along the radial direction for both the charged species, considering the ponderomotive and coulomb electrostatic force. The laser pulse was taken as spatially and temporary Gaussian with FWHM radius and duration as 5λ and $400 \lambda/c$. The simulation disk has radius and thickness of 50λ each, comprising of 50000 annular cells. The simulation disk has been filled with fully ionized helium gas of uniform electron density 1×10^{19} cm^{-3}, i.e. the typical density of the plasma present over the region developing the black central line. The boundary conditions were reflective and open for the particles at the inner ($r = 0$ µm) and outer ($r = 50$ µm) boundary respectively. The time step of the simulation has been taken as one in 200 parts of laser time period. The simulation was carried out for 20 picoseconds, where the peak of the laser pulse is reached at 2 ps.

The temporal evolution of the radial electric field profiles and the densities of both charged species, obtained from the simulations are shown in Figure 5. We see the effect of the ponderomotive force of the laser, i.e. the radial electron expulsion, during its presence followed by the generation of the ambipolar radial electric field over the region of ion 'wall' created by the coulomb explosion. The radial electric field, obtained from the simulation, during the presence of the laser pulse agrees well with the analytical expression given by Equation (1).
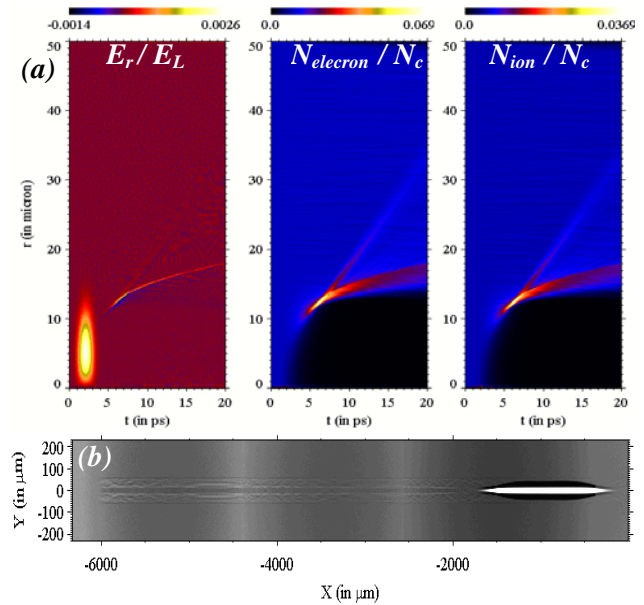

Figure 5. (a) The temporal evolution of the radial electric field, electron and ion densities obtained from the 1D cylindrical PIC code (b) The PTRACE image of the channel having the above radial electric field, where the time axis is converted to X axis, by the formula, x=ct.

We used the result for the electric field obtained from the simulation in the PTRACE code, in order to carry out a direct comparison with the proton images obtained from the experiment. In this case we converted the time axis of the electric field profile into a spatial axis by multiplying it with the speed of light, c, in the free space. The simulated proton images thus obtained from the PTRACE simulation are shown in the bottom row of Figure 5. The reproducibility of all the three features observed the experimental data confirm the physical significance of the adopted analysis and the understanding of the dominant mechanisms involved during the early stage of the interaction of the laser.

In order to obtain more complete modeling of the interaction, the problem was simulated with a 2D electromagnetic PIC code. The simulation box consisted of 6500x800 grids and 50 millions of particles in total (includes both electrons and ions), which corresponded at the initial time to 9 particles/cell (for each species) in the plasma. The spatial and temporal steps were 0.1 λ and 0.05 λ/c. The inhomogeneous, fully ionized helium plasma was modeled as starting from x = 25λ with a linear ramp up to x = 425λ, where the density reaches its maximum, equal to 0.1 times the critical density. At x = 600λ the density was dropped down to zero for numerical reasons. The laser pulse had Gaussian profiles both longitudinally and transversely. Its FWHM length and width was 150λ and 8λ respectively. The dimensionless peak amplitude was 1.9, corresponding to an intensity of 1.5×10^{19} W/cm^2.

Figure 6 shows the electric field, ion and the charge density obtained from the 2D simulation. As we can see, the simulations also provide the evidence of the ambipolar electric field profile at the channel boundary, after the end of the laser pulse. Therefore, it is concluded that the coulomb explosion of the ions in the channel and the return of hot electrons after the laser pulse, produce a waveguide pattern, with a neutral, very low density plasma medium at the core.
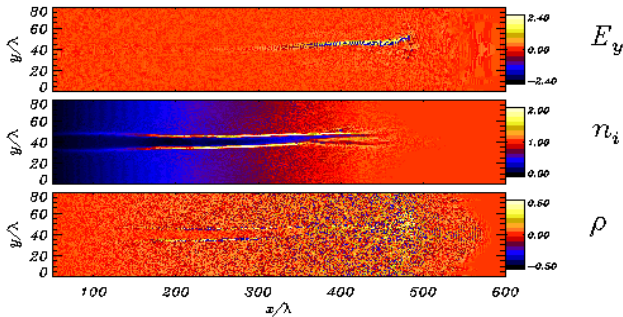

Figure 6. The transverse electric field, charge and ion densities obtained from the 2D PIC simulations at time equals to 225 laser periods. The Electric field is in the unit of the laser electric field at $a_0=1$. The charge density is in the unit of peak background density, i.e. $n_0 = 0.1\ n_c$.
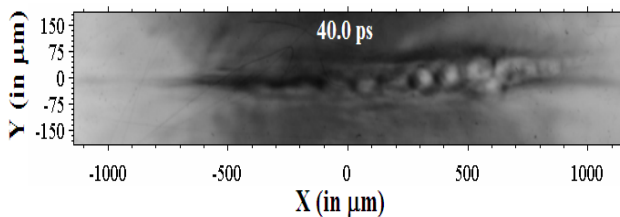
(ii) Late time developments

Figure 7. The proton image of the interaction taken at 40 ps after the arrival of the short pulse at x=0 obtained in the same shot as Figure 3(c).

From 6-8 ps after the end of the short pulse, we observed the development of quasi-periodic modulations in the channel, inside the white region bounded by dark lines. These features evolved into circular structures which were observed to decay on hydrodynamic time scales. The typical picture of the data showing this type of modulations is provided in Figure 7. There are several possible explanations for the generation of quasi static electro-magnetic fields originating this type of structures in the proton probe profile. Relativistic soliton formation is one among these. In the strong nonlinear medium, these solitions are formed due to the trapping of the red shifted electromagnetic radiation by the ambient plasma, which behaves as over-dense for them. Due to the ponderomotive force, they expel the electron from the core producing a positively charged sphere, which can be imprinted over the RCF as a 'whiter' region, similar to that observed experimentally. Studies of the relativistic soliton formation, via PIC simulations, demonstrate that they are produced deep inside the plasma slab, close to the depletion length of the laser[17]. Although the detailed investigation is under progress, we found that the theoretical estimation for the depletion length of the laser for different plasma densities, $l_{dep} = l_{pulse}\ n_c/n_e$, agrees with the experimental data.

Conclusions

In conclusion, we have reported the first, direct, experimental observation of the charge dynamics following high power laser interaction with under-dense plasma, via the proton imaging technique. The formation of an electron depleted channel under the effect of the laser ponderomotive force and the following coulomb explosion of the ions are unambiguously interpreted by 1D and 2D PIC simulations followed by Particle tracing.The physical interpretation for interesting features observed at later times inside the channel is currently under progress.

References

1. C.G.R. Geddes, *et al.*,
   Nature, <u>431</u>**,** 538 (2004)

2. J. Faure, *et al.*,
   Nature, <u>431</u>**,** 541 (2004)

3. S.P.D. Mangles, *et al.*,
   Nature, <u>431</u>**,** 535 (2004)

4. K. Nakajima, *et al.*,
   Phys. Rev. Lett., <u>74</u>**,** 4428 (1995)

5. F. Amiranoff, *et al.*,
   Phys. Rev. Lett., <u>74</u>**,** 5220 (1995)

6. A. Modena, *et al.*,
   Nature, <u>377</u>**,** 606 (1995)

7. M. Borghesi, *et al.*,
   Laser and Particle Beams, <u>18</u>**,** 389 (2000)

8. M. Borghesi, *et al.*,
   Phys. Rev. Lett., <u>83</u>**,** 4309 (1999)

9. M. Borghesi, *et al.*,
   Phys. Rev. Lett., <u>78</u>**,** 879 (1997)

10. G.S. Sarkisov, *et al.*,
    Phys. Rev. E, <u>59</u>**,** 7042 (1999)

11. G.S. Sarkisov, *et al.*,
    Plasma Phys. Reports, <u>66</u>**,** 787 (1997)

12. M. Borghesi, *et al.*,
    Rev. Sci. Instrum., <u>74</u>**,** 1688 (2003)

13. M. Borghesi, *et al.*,
    Phys. Rev. Lett., <u>92</u>**,** 55003 (2004)

14. R. Jung, *et. al.*, pg. 23 *in this report.*

15. E. Esarey, *et al.*,
    IEEE J. Quant. Electron., <u>33</u>**,** 1879 (1997)

16. P. Sprangle, *et al.*,
    Phys. Rev. Lett., <u>64</u>**,** 2011 (1990)

17. S.V. Bulanov, *et al.*,
    Phys. Rev. Lett., <u>82</u>**,** 3440 (1999)